PCCP

Accepted Manuscript

ROYAL SOCIETY OF CHEMISTRY

www.rsc.org/pccp

Journal Name

ARTICLE

Synthesis of ZnO nanosheets arrays with exposed (100) facet for gas sensing applications

Received 00th January 20xx,
Accepted 00th January 20xx

DOI: 10.1039/x0xx00000x
www.rsc.org/

Chuanhai Xiao, Tianye Yang, Mingyan Chuai, Bingxin Xiao and Mingzhe Zhang*

ZnO nanosheets (NSs) arrays have been synthesized by a facile ultrathin liquid layer electrodeposition method. The ion concentration and electrode potential play important roles in the formation of ZnO NSs arrays. Studies on the structural information indicate that the NSs are exposed with (100) facet. The results of Raman and PL spectra indicate that there existed a large amount of oxygen vacancies in the NSs. The gas sensing performances of the ZnO NSs arrays are investigated: the ZnO NSs arrays exhibited high gas selectivity and quick response/recovery for detecting NO_2 at a low working temperature. High binding energies between NO_2 molecules and exposed ZnO (100) facets lead to large surface reconstructions, which is responsible for the intrinsic NO_2 sensing properties. In addition, the highly exposed surface and large amount of oxygen vacancies existing in the NSs also make a great contribution to the gas sensing performance.

1 Introduction

Zinc oxide, a promising n-type semiconductor, has been applied in many fields, such as gas sensors, photocatalysts, optoelectronic devices and solar cells.[1-4] As one of the competitive candidates for applications in gas sensors due to its advantages of high sensitivity, stability and low-cost, ZnO nano-structure has already been widely used for detecting gases such as CO, NO_2, and ethanol.[5-10] With the progress of gas-sensing research, it has been found that nanostructures with the high surface area and surface accessibility can significantly improve the gas-sensing properties, and thus plenty of attention has been focused on the preparation of ZnO nanostructures.[5] Small size ZnO nanoparticles exhibit excellent gas sensing properties due to their high specific surface area and activity. However, the inevitable aggregation of the nanoparticles hinders the diffusion of gases into the inner part of the secondary particles, which will eventually worsen and delay the response. Recently, 2D ZnO nanostructures such as nanosheets, nanowalls, and nanoplates have attracted particular attention for gas sensing property because of their high surface to volume ratios and the comparable of lateral dimensions and the thickness of the surface space-charge region.[7,11] The synergic combination of the two effects can make it with high detection efficiencies at low operating temperature, fast response and recovery capability. Thus, the 2D ZnO nanomaterials are widely applied as efficient components of some efficient gas sensors to participate in the detection of various hazardous and toxic gases. Until now, only a few reports have been made for the synthesis of 2D ZnO nanostructures grown by different fabrication techniques.

It is generally recognized that the performances of solid state gas sensors are directly dependent on the surface state and morphology of the sensing materials.[12,13]. Theoretical and experimental results indicate that nanosized materials can exhibit special features corresponding to their nanostructures encased in specific facets.[8,11,14-16] Recently, there has been a growing interest in the synthesis of nanostructures with specifically exposed crystal surfaces and in the exploration of their crystal plane-dependent properties for applications such as gas sensors and catalysts.[8,11,12] As well known, the gas sensing behaviour of metal-oxide semiconductor is mainly dominated by interactions between the target gas and the sensing surface, which brings about a resistance change. Hence, gas sensors exhibit different surface properties (such as defect concentration, surface modification and exposed facets), which could lead to varying gas sensing performance.

Activated by the above mentioned, ZnO NSs arrays were prepared by an electrochemical deposition self-assembly approach in a quasi-two-dimensional ultra-thin liquid layer. The single-crystalline ZnO NSs are exposed with (100) facet and there are existed amount of oxygen vacancies. The thickness of NSs is about 20 nm, which is comparable to the Debye length. The as-obtained ZnO NSs arrays are developed for the detection of NO_2 gas which exhibit high selectivity, short response and recovery time. In addition, the gas-sensing mechanism of such excellent sensing performance is discussed.

2 Experimental

2.1 Synthesis of ZnO NSs arrays

State Key Laboratory of Superhard Materials, Jilin University, Jilin 130012, China.
** Corresponding author E-mail address: zhangmz@jlu.edu.cn*

All the chemicals were analytical grade reagents without further purification. The electrolyte solution of 0.04 M $Zn(NO_3)_2$ was prepared by Millipore water. The growth system consisted of a growth chamber, a low temperature cycle water bath, a DC power supply (DF1731SB5A), an arbitrary function generator (AFG 310), an optical microscope (Leica Dmlm) and a CCD camera (A311f). A Peltier element attached to DC power supply was fixed in the center of the growth chamber, which was used to rapidly adjust the electrolyte temperature. The growth chamber temperature was controlled by low-temperature cycle water bath, and the growth potential was supplied by an arbitrary function generator. The growth process could be observed by the optical microscope and CCD camera.

Firstly, silicon substrates (WaterNet Co., Type N, 0.5 mm thick, orientation [100], resistivity 2-5 Ω/cm) were cut into pieces about 20 × 20 mm^2 before using, And secondly, they were completely cleaned with acetone, chloroform, ethanol, and Millipore water for 10 min respectively in the ultrasonic circumstance and then blown dry with high-purity nitrogen. Finally, they were treated with an oxygen plasma for 3 min at 300 W (Templa System 100-E plasma system) and rinsed again with Millipore water. The surface of silicon substrates became fully hydrophilic after above procedure. Surface structures with $-CH_3$ termination were carried out by immersing the silicon substrate into a 1mm OTS (APTMS, Aldrich) solution of 1-phenyloctane (Aldrich) or hexadecane (Aldrich) for 15 min in the ultrasonic condition, and then were rinsing in chloroform to remove the polymeric residuals. Subsequently, the silicon wafer was placed on the Peltier element while two parallel electrodes made of a 30 μm thick Zn foil were put on silicon substrates and separated by a distance of approximately 8 mm. Then the solution was dropped on the silicon substrate. Finally, a cover glass was carefully put on the two electrodes and then filled the space between the cover glass and silicon substrate with solution. A uniform ultra-thin ice layer could be formed between the silicon substrate and cover glass by adjusting the temperature of the Peltier element and the low-temperature cycle water bath. After an ultra-thin ice layer was formed, we kept the growth chamber temperature constant for 30 min. The ultrathin liquid layer of concentrated electrolyte was formed between the ice layer and upper surface of silicon substrate, as well as the ice layer and lower surface of cover glass. Electrodeposition was initiated when a constant voltage of 0.8 V was applied on the parallel electrodes. As the growth process ended, a slight increase in temperature was provided by the Peltier element to melt ice. Then the cover glass and silicon substrate were taken out to clean by the deionized water and dried at room temperature. The growth process was displayed in the supplementary information.

2.2 Characterization and gas-sensing measurement

The morphology and crystal structure of the ZnO NSs arrays were characterized by scanning electron microscope (SEM FEI Magellan-400), X-ray diffraction (XRD, Rigaku D/max-Ra) and transmission electron microscopy (TEM, JEOL JEM-2200FS) respectively. Transmission spectra were recorded on the HR-800 Lab Ram Infinity spectrophotometer which was carried out with a continuous He-Cd laser with the excitation wavelength of 325 nm and UV-3150 spectrophotometer, respectively. Room temperature Raman spectrum and PL spectrum were recorded on a HR-800 LabRam Infinity spectrophotometer excited by a continuous He-Cd laser with respective excitation wavelengths of 325 nm.

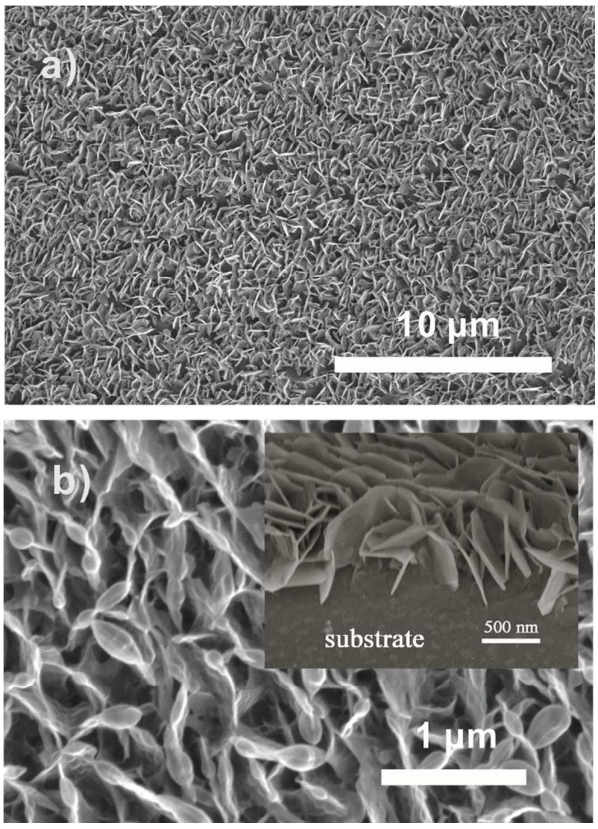

Fig. 1 (a) Low- and (b) High-magnification SEM images of ZnO NSs arrays. The insert is the cross-sectional view of the NSs arrays.

The samples on the cover glass were used as the test objects. At first, the samples were covered by a linear mask with a width of 50 μm. Two copper wires were fixed on both sides of the mask separately. Then the Au film was deposited on the glass by vacuum ion sputtering for 300 s. After that, the mask was taken away, and the NSs arrays were connected into the circuit. During the measurement, the electrical signals were measured and recorded by a Keithley 2400 sourcemeter (2400, Keithley, USA) and a Digital Phosphor Oscilloscope (TDS5034B, Tektronix, USA). The working temperature was controlled by a flat heating plate with a temperature controller. The desired concentrations of the testing gases were obtained by the static gas distribution method, which was calculated by the following formula:[5]

$$Q = \frac{V \times \phi \times M}{22.4 \times d \times \rho} \times 10^{-9} \times \frac{273 + T_R}{273 + T_B} \quad (1)$$

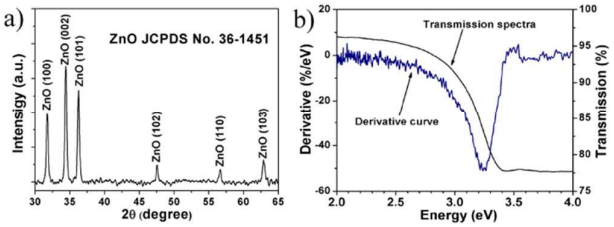

Fig. 2 (a) XRD pattern of ZnO NSs arrays. (b) Transmission spectra (black line) and the corresponding derivative curves (blue line) of ZnO NSs arrays.

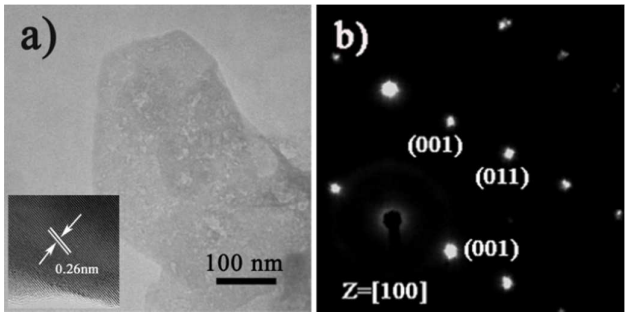

Fig. 3 (a) TEM and b) SEAD images of the individual ZnO NS. The inset shows the corresponding HR-TEM pattern.

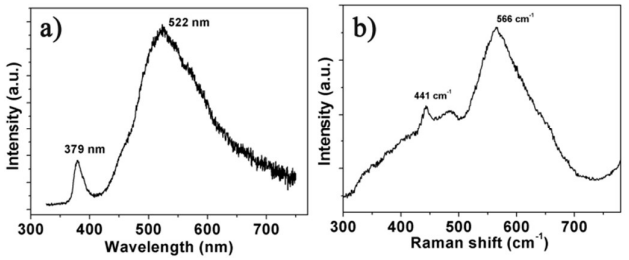

Fig. 4 (a) PL and (b) Raman spectra of the ZnO NSs film.

where Q (mL) is the liquid volume of the volatile compound or gas volume; V (mL) is the volume of the testing chamber; ϕ (ppm) is the required gas volume fraction; M ($g \cdot mol^{-1}$) is the molecular molar mass; d ($g \cdot cm^{-3}$) is the specific gravity, and ρ is the purity of the volatile testing liquid or gas; T_R and T_B (°C) are the temperatures at ambient and test chamber, respectively. The sensor response (R) is defined as the relative conductance (resistance) variation upon exposure to reducing (oxidizing) target gases, respectively.[3] The gas sensing measurements are carried out at a relative humidity (RH) 30% at 25 °C. The response time is defined as the time it take for a sensor to reach 90% of its saturation value after it is exposed to detected gases, and the recovery time is the time for recovery of the resistance to 90% of the initial level after exposure to air. The uncertainty of gas sensing test is mainly induced by the electrode connection process.

3 Results and Discussion

3.1 Structure, morphology and optical properties

Fig. 1a and b display the SEM images of ZnO NSs arrays with low and high magnification, and the insert image (in Fig. 1b) displays the cross-sectional view of the NSs arrays. The images illustrate that the ZnO array is interwoven by abundant NSs with an average thickness of 20 nm. The unique NSs arrays with external inter-space between each NS can provide an extensive pore network for gas diffusion.

To gain the component and structure information of ZnO NSs arrays, XRD, TEM and spectrum experiments were conducted. The XRD pattern of ZnO NSs arrays is shown in Fig. 2a. All the diffraction peaks match to those characteristic of the wurtzite ZnO structure (JCPDS 036-1451). No characteristic peaks of other chemical compounds were observed such as Zn or $Zn(OH)_2$, indicating that the electrodeposition product is pure ZnO. Fig. 2b depicts the transmission spectrum and its derivative curve of the ZnO NSs arrays. Only one distinct peak is observed at about 3.24 eV in derivative curves, which arises from the ZnO near-band-edge (NBE) absorption. Further structural characterizations of the as-synthesized nanodeposits were performed with TEM. Fig. 3a shows a TEM image of the individual ZnO NS. The HR-TEM analysis of an individual NSs (the inset of Fig. 3a) reveals that clear lattice fringes with a lattice spacing of 0.26 nm corresponds well to the d-spacing of the (002) plane of the hexagonal wurtzite ZnO. The selected area electron diffraction (SAED) pattern of the ZnO NSs shown in Fig. 3b can be indexed to the (100) zone axis of single crystal hexagonal wurtzite ZnO. On the basis of the above observations and structural analysis, we can conclude that the exposed surfaces of the as-prepared ZnO NSs are (100) facets.

The gas-sensing mechanism of semiconductor gas sensors is generally based on the adsorption and reaction of gas molecules on the material surface, where oxygen deficiency plays an important role. Usually, the Raman and PL spectra are carried out to analyse the defects of semiconductor materials due to their higher sensitivity to crystal imperfections. Fig. 4a displays that the typical PL spectrum indicating two bands at 379 and 522 nm. The ultraviolet (UV) peak nears 380 nm can be attributed to the conduction band to valence band (CB-VB) combination according with the result of transmission spectrum in Fig. 2b. The green PL near 500 nm is usually ascribed to oxygen vacancy and the yellow or orange PL (near 600 nm) is related to oxygen interstitial.[17] Two peaks of Raman spectrum at 441 and 566 cm^{-1} shown in Fig. 4b are assigned to the E_{2H}, and E_{1L} vibrational modes of the ZnO, respectively. The E_{2H} mode involves oxygen atoms, and the E_{1L} mode is associated with oxygen deficiency indicating that oxygen vacancies exist in the NSs[18]. The broad features of 566 cm^{-1} peak in the Raman spectra and the high intensity 500 nm band in the PL spectrum indicate that ZnO NSs are significantly deficient in oxygen.[17,18] According to the above analyses, there exists large amounts of oxygen vacancies in the ZnO NSs arrays.

3.2 Gas-sensing properties

Based on as-prepared ZnO NSs arrays, we fabricate chemical sensors and investigate their gas sensing performances. The

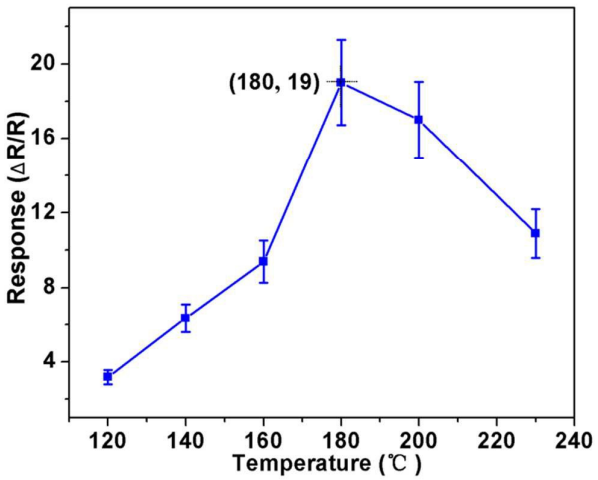

Fig. 5 Gas response of ZnO NSs film to 100 ppm NO_2 as the function of the operating temperatures.

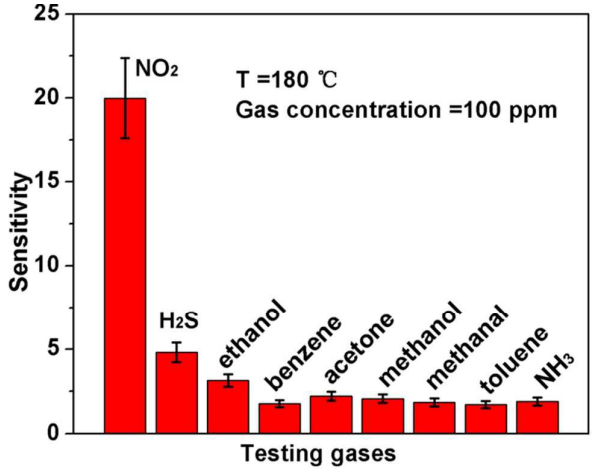

Fig. 6 Responses of ZnO NSs film to 100 ppm various testing gases.

gas-sensing properties are heavily affected by the working temperature, as this factor greatly influences the surface state of sensing materials. Therefore, in order to investigate the influence of the operating temperature and to find an optimum operating temperature of the sensors, the sensitivities of the as-prepared ZnO nanostructures toward 100 ppm of NO_2 as a function of working temperature are tested and the results are shown in Fig. 5. It can be observed that the sensitivity of the ZnO NSs sensor increases gradually while the working temperature rises from 120 to 180 °C and reaches a maximum value of R= 20 at 180 °C. A further increase of the operating temperature above 180 °C, however, results in a gradual decline in the sensitivity of the sensors. Thus, the operating temperature of 180 °C is the optimal temperature for NO_2 detection, so it is chosen as the working temperature to further examine the characteristics of the sensor. Compared with the NO_2-sensing properties of other ZnO-based nanostructures[19-22], sensor in this work exhibits lower or comparable working temperature.

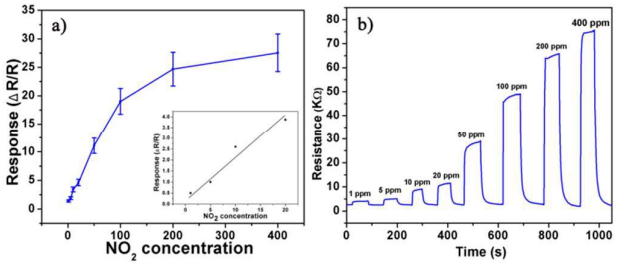

Fig. 7 (a) Gas response of ZnO NSs film to 100 ppm NO_2 as the function of the operating temperatures. The inset is the I-V characteristics of the ZnO NSs under NO_2 and air. (b) Typical dynamical response of ZnO NSs arrays upon exposure to square concentration pulses of NO_2.

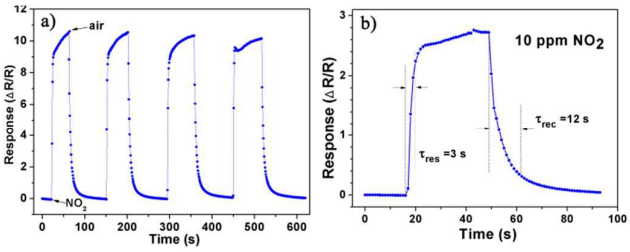

Fig. 8 (a) Dynamic responses to NO_2 of the sensors to NO_2 (50 ppm). (b) The response transient of the ZnO based sensors to 10 ppm NO_2 at 180 °C.

Besides, we further examine other gas-sensing properties including selectivity, detection limit, stability, response and recovery time, which are important parameters for the gas sensor in practical applications. Fig. 6 shows the selectivity of the ZnO NSs sensors to NO_2 relative to H_2S, ethanol, benzene, acetone, methanol, methanal, toluene and NH_3 at the same gas concentrations (100 ppm). The gas sensing response to NO_2 is much higher than other gases, suggesting that the obtained ZnO NSs arrays have high selectivity for NO_2. Fig. 7a illustrates that the responses of sensor based on ZnO NSs as a function of NO_2 concentration from 1 to 400 ppm. In the low concentration range from 1 to 100 ppm, we observe that the sensitivity is approximately linear increase with increasing NO_2 concentration (shown in the insert of Fig. 7a). Above 100 ppm, the sensitivity changes slowly with the variations of the NO_2 concentration, which indicates that the sensor is near saturation. Furthermore, the stability of the gas sensors is also a crucial point for the practical application of the gas sensors. Fig. 7b depicts the representative dynamic responses to different NO_2 concentrations (1-400 ppm) at 180 °C, respectively. The response transient of ZnO NSs sensor to 50 ppm NO_2 is shown in Fig. 8a. The four sequential cycles of response transients show that a reversible, repeatable and stable characteristic. The transient response of ZnO NSs to 10 ppm NO_2 is shown in the inset of Fig. 8b. The results indicate that the sensor responds immediately when NO_2 gas is introduced and then rapidly recovers to initial value after the NO_2 releasing. The respective response and recovery times of ZnO NSs sensors are around 3 and 12 s. Compared with the NO_2 sensing properties of other ZnO-based nanosystems[19-24], sensor in this work exhibits comparable or wider detection limits but faster response and recovery time, which is due to

the specific structure of these ZnO NSs with a greater surface area and highly exposed surface.

3.3 NO_2-sensing mechanism

It is crucial to understand the sensing mechanism for designing NO_2 sensors of high sensing performances. As metal oxide ZnO exposed to air, oxygen molecules will be adsorbed on the oxide surface and then extract electrons in the bulk, leading to a narrow conduction channel. When the n-type semiconductor ZnO is exposed to NO_2 gas the NO_2 molecules can not only capture electrons from the ZnO conduction band but also react with the chemisorbed oxygen on the surface, which results in withdrawing of electrons from the surface, depleting them from the conduction band, and leading to an increase in resistance (Eq. 2 and 3). When the semiconductor oxide is exposed to air again, NO_2^- reacts with hole release electrons into the conduction band, leading to NO_2 being released into the air and reducing resistance (Eq. 4). The adsorption and desorption occur on the ZnO surface according to the following chemical reaction:[6]

$$NO_2(gas)+e^- \rightarrow NO_2^-(ads) \quad (2)$$

$$NO_2(gas)+O_2^-(ads)+2e^- \rightarrow NO_2^-(ads)+2O^-(ads) \quad (3)$$

$$NO_2^-(ads)+h^+ \rightarrow NO_2(gas) \quad (4)$$

The kinetics process of gas adsorption and desorption can be understood as follows: When the NO_2 gas flows through the sensor element, the adsorption speed of NO_2 on the sensor surface is very fast, indicated by the steep slope of the response process. This suggests that the adsorption process plays a dominant role during the initial sensing stage. As the sensing process goes on, the adsorption of the NO_2 gas slows down gradually. When the gas adsorption and desorption reach equilibrium, the resistance increases to the maximum value. In contrast, desorption of NO_2 gas dominates the sensing process when the NO_2 flow is stopped, resulting in the return of the sensor signal to the baseline.

The electron exchange between the surface states and the bulk takes place within a surface layer whose width is about λ_D (Debye length). The value of λ_D can be calculated by the following equation:[25]

$$\lambda_D = \left(\frac{\varepsilon kT}{q^2 n_c}\right)^{1/2} \quad (5)$$

where ε is the static dielectric constant; κ is the Boltzmann's constant; T is the absolute temperature; q is the electrical charge of the carrier and n_c is the carrier concentration. For bulk ZnO, λ_D is about 20 nm at 180 °C according to the above equation as n_c is assumed to be 5×10^{16} cm^{-3}. Thus, the thickness of the ZnO NSs is comparable to the Debye length which could effectively enhance the gas sensing performance. It is recognized that the reaction of NO_2 on gas sensing materials is expected to occur mainly via electron transfer and variation of oxygen species on the surface. Considering that the electrical properties of the semiconductor oxides are significantly influenced by the native defects or the nonstoichiometry. Chemisorbed NO_2 binds more strongly to the oxygen vacancy site, which exist on the ZnO (100) surface, with higher binding energies greater than clean stoichiometric ZnO (100) surface. Large surface reconstructions around the oxygen vacancy site can take place after NO_2 adsorption, which can lead to large electrical resistance variation.[26] On the other hand, such a rapid sensing performance can be ascribed to be the special NSs arrays structure in which the gas adsorption and desorption would be remarkably improved by the highly exposed internal spaces among the NSs. Meanwhile, most of the active sites in the sensing layer consists of ZnO NSs can be effectively utilized for contact reactions, resulting in remarkably improved response, lower working temperature and shorter response and recovery time.

4 Conclusions

The hierarchical ZnO arrays assembled from 2D NSs with exposed (100) facets are synthesized through a facile ultrathin liquid layer electrodeposition method. PL and Raman spectra gas-sensing results reveal that the NSs-assembled ZnO arrays exhibit excellent NO_2 gas sensing performance evidenced by high response, small cross sensitivity, fast response/recovery (3 s and 12 s) and low operating temperature (180 ^oC), suggesting their potential applications as advanced gas sensing materials. The excellent performance in sensing can be attributed to the specific morphology of the NSs arrays and the thin NSs exposed with (100) facet. In addition, there exists amount of oxygen vacancies in ZnO NSs which is benefit for its gas sensing performance. This present work will provide a deeper understanding of the sensing mechanism of ZnO-based sensors, and motivates us to further fabrication of other nanomaterials with specially exposed crystal surfaces for promising applications in gas sensors, photocatalysts and more.

Acknowledgements

This work was funded by the National Science Foundation of China, No. 11174103, 11474124, and the Graduate Innovation Fund of Jilin University, No. 2015132.

Notes and references

1 D. Barreca, D. Bekermann, A. Devi, R. A. Fischer, A. Gasparotto, C. Maccato, E. Tondello, M. Rossi, S. Orlanducci and M. L. Terranova, *Chem. Phys. Lett.*, 2010, **500**, 287-290.

2 D. Barreca, D. Bekermann, E. Comini, A. Devi, R. A. Fischer, A. Gasparotto, C. Maccato, G. Sberveglieri and E. Tondello, *Sen. Actuators, B*, 2010, **149**, 1-7.

3 D. Barreca, D. Bekermann, E. Comini, A. Devi, R. A. Fischer, A. Gasparotto, C. Maccato, C. Sada, G. Sberveglieri and E. Tondello, *Cryst. Eng. Comm*., 2010, **12**, 3419-3421.

4 L. Schmidt-Mende and J. L. MacManus-Driscoll, *Mater. Today*, 2007, **10**, 40-48.

5 Y. Zeng, L. Qiao, Y. Bing, M. Wen, B. Zou, W. Zheng, T. Zhang and G. Zou, *Sen. Actuators, B*, 2012, **173**, 897-902.

6 R. Kumar, O. Al-Dossary, G. Kumar and A. Umar, *Nano-Micro Lett.*, 2015, **7**, 97-120.

7 F. Fan, P. Tang, Y. Wang, Y. Feng, A. Chen, R. Luo and D. Li, *Sen. Actuators, B*, 2015, **215**, 231-240.

8 J. Liu, X. Chen, W. Wang, Y. Liu, Q. Huang and Z. Guo, *Cryst. Eng. Comm*., 2011, **13**, 3425-3431.

9 V. Saxena, D. K. Aswal, M. Kaur, S. P. Koiry, S. K. Gupta, J. V. Yakhmi, R. J. Kshirsagar and S. K. Deshpande, *Appl. Phys. Lett.*, 2007, **90**, 043516.

10 C. W. Na, H.-S. Woo, I.-D. Kimb and J.-H. Lee, *Chem. Commun.*, 2011, **47**, 5148-5150.

11 Y. Xiao, L. Lu, A. Zhang, Y. Zhang, L. Sun, L. Huo and F. Li, *ACS Appl. Mater. Interfaces*, 2012, **4**, 3797-3804.

12 S. Bai, K. Zhang, L. Wang, J. Sun, R. Luo, D. Li and A. Chen, *J. Mater. Chem. A*, 2014, **2**, 7927-7934.

13 Y. V. Kaneti, Z. Zhang, J. Yue, Q. M. Zakaria, C. Chen, X. Jiang and A. Yu, *Phys. Chem. Chem. Phys.*, 2014, **16**, 11471-11480.

14 Z. Lai, F. Peng, H. Wang, H. Yu, S. Zhang and H. Zhao, *J. Mater. Chem. A*, 2013, **1**, 4182-4185.

15 X. Han, M. Jin, S. Xie, Q. Kuang, Z. Jiang, Y. Jiang, Z. Xie and L. Zheng, *Angew. Chem.*, 2009, **121**, 9344-9347.

16 G. Cui, Z. Li, L. Gao and M. Zhang, *Phys. Chem. Chem. Phys.*, 2012, **14**, 16321-16325.

17 K. K. Naik, R. Khare, D. Chakravarty, M. A. More, R. Thapa, D. J. Late and C. S. Rout, *Appl. Phys. Lett.*, 2014, **105**, 233101.

18 D. Li, Y. H. Leung, A. B. Djurišić, Z. T. Liu, M. H. Xie, S. L. Shi, S. J. Xu, and W. K. Chan, *Appl. Phys. Lett.*, 2004, **85**, 1601-1603.

19 J. H. Jun, J. Yun, K. Cho, I.-S. Hwang, J.-H. Lee and S. Kim, *Sen. Actuators, B*, 2009, **140**, 412-417.

20 D Calestani, M Villani, R Mosca, L Lazzarini, N Coppedè, S C Dhanabalan and A Zappettini, *Nanotechnology*, 2014, **25**, 365502.

21 L. Shi, A. J. T. Naik, J. B. M. Goodall, C. Tighe, R. Gruar，R. Binions, I. Parkin and J. DarrM. *Langmuir*, 2013, **29**, 10603-10609.

22 F. Fan, Y. Feng, S. Bai, J. Feng, A. Chen and D. Li, *Sen. Actuators, B*, 2013, **185**, 377-382.

23 F.-T. Liu, S.-F. Gao, S.-K. Pei, S.-C. Tseng and C.-H. J. Liu, *J. Taiwan Inst. Chem. E,* 2009, **40**, 528-532.

24 J. X. Wang, X. W. Sun, Y Yang and C. M. L. Wu, *Nanotechnology*, 2009, **20**, 465501.

25 C. L. Zhu, Y. J. Chen, R. X. Wang, L. J. Wang, M. S. Cao and X. L. Shi, *Sen. Actuators, B*, 2009, **140**, 185-189.

26 M. Breedon, M. J. S. Spencer and I. Yarovsky, *J. Phys. Chem. C*, 2010, **114**, 16603-16610.